Coexisting Edge States and Gapless Bulk in Topological States of Matter

Yuval Baum,[1] Thore Posske,[2] Ion Cosma Fulga,[1] Björn Trauzettel,[2] and Ady Stern[1]
[1]*Department of Condensed Matter Physics, Weizmann Institute of Science, Rehovot 76100, Israel*
[2]*Institut für Theoretische Physik und Astrophysik, Universität Würzburg, 97074 Würzburg, Germany*
(Received 28 November 2014; published 31 March 2015)

We consider two-dimensional systems in which edge states coexist with a gapless bulk. Such systems may be constructed, for example, by coupling a gapped two-dimensional state of matter that carries edge states to a gapless two-dimensional system in which the spectrum is composed of a number of Dirac cones. We find that, in the absence of disorder, the edge states could be protected even when the two systems are coupled, due to momentum and energy conservation. We distinguish between weak and strong edge states by the level of their mixing with the bulk. In the presence of disorder, the edge states may be stabilized when the bulk is localized or destabilized when the bulk is metallic. We analyze the conditions under which these two cases occur. Finally, we propose a concrete physical realization for one of our models based on bilayer Hg(Cd)Te quantum wells.

DOI: 10.1103/PhysRevLett.114.136801 PACS numbers: 73.20.At, 03.65.Vf, 73.21.Fg, 73.43.Cd

Introduction.—The classification and realization of topological states of matter are among the main themes in modern condensed matter physics [1–3]. Of particular interest are topological insulators and topological superconductors, which have drawn a great deal of attention over the past few years [4–14]. The bulk of these states is gapped, but the edge is commonly gapless. The gapless edge modes are protected from backscattering and localization either by chirality or by symmetry.

In this work, we present several examples of two-dimensional models that simultaneously host one-dimensional gapless modes on the edge and are gapless in the two-dimensional bulk. The edge states possess unique properties that distinguish them from nontopological edge states. Most notably, they are either chiral or helical and intimately related to properties of the bulk. In the absence of disorder, these models all share similar spectral and transport characteristics, showing distinct bulk and edge contributions that do not mix. In contrast, the effect of disorder unravels the difference between them. In some of the models, disorder stabilizes the edge modes and decouples them from the bulk, while in others it completely mixes the two. Similarly, the different nature of the different models is revealed when we introduce weak perturbations that open energy gaps in the spectrum. We provide concrete Hamiltonians based on coupling a gapless phase to a topological phase—for example in a bilayer system—and analyze their spectral and transport properties. Beyond that, we present a concrete physical realization based on a bilayer Hg(Cd)Te quantum well. Note that the systems we consider share the lack of bulk energy gaps with Weyl semimetals and nodal superconductors [15,16], but these systems are distinguished from them by being two dimensional and by having no topological protection against the gapless nature of the bulk.

The edge properties in gapped topological states of matter can be studied through the local density of states (LDOS) [3,11–13]. At energies smaller than the bulk energy gap, the LDOS is nonzero at the edge and decreases exponentially as a function of the distance from the edge. Because of the absence of a bulk gap, this is not the case for the systems we consider, and we therefore have to employ different methods for studying the edge. For the clean case, we study a cylindrical geometry in which the lattice momentum parallel to the edge, $k_\parallel$, commutes with the Hamiltonian. We find two types of edge states, which we call strong and weak. Strong edge states carry a momentum $k_\parallel$ and an energy $\epsilon(k_\parallel)$ for which there are no bulk states. Consequently, their wave functions are exponentially localized near the edge, with the localization length being inversely proportional to the bulk gap at $k_\parallel$. Weak edge states occur when, for all values of $k_\parallel$ and energies $\epsilon(k_\parallel)$ for which there are states at the edge, there are also states in the bulk. The edge states then hybridize with the bulk states, and their wave functions are not exponentially localized. We find that the "strength" of the edge mode depends on the orientation of the edge.

The edge states are also reflected in transport [3,9–12,14]. We distinguish between edge versus bulk transport by studying transport in devices of two terminals with both periodic and hard wall boundary conditions. This method is also useful in the presence of disorder, where states are not characterized by momentum. Generally, in gapped phases with a nontrivial topological index, edge state transport is robust as long as the relevant energy scales for transport are smaller than the bulk gap. Remarkably, for the systems we consider, the bulk gap vanishes, and yet the edge state transport may still be robust. In particular, we find that disorder may even stabilize the edge state transport.

The effect of disorder on the systems we consider may be inferred from the effect of a translationally invariant perturbation that opens a gap in the bulk spectrum. Such a perturbation makes the system acquire a well-defined topological index. When the topological index is a Chern number whose value does not depend on the perturbation that opens the gap, the gapless phase is a transition between two insulating phases with the same Chern number. Then, in the presence of disorder, the bulk states may become localized and the edge states stabilize. In contrast, when the value of the Chern number depends on the sign of the perturbation, then the gapless phase separates topologically distinct insulating phases and the phase diagram in the space of disorder and gap-opening perturbation must contain a critical line where the bulk states remain delocalized and the edge states disappear. Away from the critical line, the system is a well-defined Chern insulator. For cases where the topological index is not a Chern number, the localization properties of the bulk and edge states depend on the symmetries of the specific model.

We now introduce four models that share the same behavior in the absence of disorder—namely, a coexistence of edge states and gapless bulk—but strongly differ away from that point. The models we consider are based on a designed coupling between a gapped two-dimensional topological phase H_1 and a gapless two-dimensional phase H_2. The simplest example would be a bilayer system in which the two layers are described by the Hamiltonians H_1, H_2 and are tunnel coupled by H_c. The combined Hamiltonian can then be written as

$$H = \begin{pmatrix} H_1 & H_c \\ H_c^\dagger & H_2 \end{pmatrix}. \tag{1}$$

Here, the topological phase H_1 is an insulator or a superconductor with a nontrivial topological index. For simplicity, we assume that the gap of H_1 is the largest energy scale. The Hamiltonian H_2 is gapless, having, for example, a Dirac spectrum. The coupling H_c is chosen such that the full Hamiltonian remains gapless. The different blocks should be combined such that the full Hamiltonian is irreducible, and hence it belongs to a symmetry class, according to Ref. [1]. In general, the symmetry class of the full Hamiltonian is given by the minimal symmetry of H_1 and H_2, although, by fine-tuning the parameters, the resulting Hamiltonian may accidentally obey additional symmetries.

In the first three models, H_1 describes a quantum Hall state with a nonzero Chern number, while H_2 describes three gapless phases that follow three different symmetries. As a consequence of the different symmetries, the effect of disorder on the three systems is markedly different. Models I and II show the behavior of a system where the value of the Chern number is independent or dependent on the gap-opening perturbation, respectively. Model III shows that the symmetries of the full Hamiltonian determine its behavior, even when the building blocks H_1 and H_2 have different localization properties. The fourth model belongs to a different topological class but has the advantage of being experimentally accessible in a bilayer Hg(Cd)Te quantum well [9,10].

Model I.—A gapped Chern insulator coupled to a two-dimensional Dirac metal. For the topological part, H_1, we take the Qi-Wu-Zhang Hamiltonian [17] of the quantum anomalous Hall effect,

$$H_1 = \sum_{\mathbf{k}} [\epsilon(\mathbf{k}) - [t_0(\cos k_x + \cos k_y) - \mu]\sigma_z + v_1(\sigma_x \sin k_x + \sigma_y \sin k_y)], \tag{2}$$

where $\epsilon(k) = t_1(1 - \cos k_x - \cos k_y)\sigma_0$ is the kinetic energy and the σ's are the Pauli matrices in spin space. Here and in the following, we set the lattice constant to $a = 1$ and $t_0 = 1$, expressing all other Hamiltonian parameters relative to these scales. The model belongs to symmetry class A and has a nonzero Chern number for $0 < \mu < 2$. For the gapless part, we use $H_2 = \sum_{\mathbf{k}} v_2(\sigma_x \cos k_x + \sigma_z \sin k_y)$, which contains four Dirac cones in its spectrum. Notice that this model obeys effective time-reversal, particle-hole, and chiral symmetries which all square to unity: $\mathcal{T} = \sigma_x\mathcal{K}$, $\mathcal{P} = \sigma_z\mathcal{K}$, and $\mathcal{C} = \sigma_y$, respectively. Therefore, it belongs to the class BDI [1], which is topologically trivial in two spatial dimensions. Finally, we take $H_c = t\sum_k(\sigma_0 + \sigma_x)$ for the coupling Hamiltonian. In fact, for any H_c with a zero determinant, the full Hamiltonian remains gapless. Solving for its spectrum in a cylindrical geometry, we find weak edges when the boundary is along the y direction or spans an angle of $\pm\arctan(0.5)$ with the x axis. The strong edge states appear for all other boundary orientations.

The band structure of the system with open boundary conditions in the y direction are shown in Fig. 1(a). The red (green) points denote right (left) propagating edge states whose wave functions decay exponentially into the bulk [Fig. 1(b)]. The zero modes in the bulk coexist with well-localized chiral edge states. In contrast, the spectrum and typical edge states of a system with open boundary conditions in the x direction are shown in Figs. 1(c) and 1(d). The red points denote edge states that hybridize with the bulk. We find numerically that the local density of states near the edge is larger than in the bulk (not shown), but the latter does not decay to zero at large distances from the edge.

Adding a mass term $m\sigma_y$ to H_2 opens a bulk gap. This term breaks both the $\mathcal{P}$ and $\mathcal{C}$ symmetries of H_2 but leaves $\mathcal{T}$ intact. Hence, the gapped version of H_2 belongs to class AI in the tenfold classification [1,2], which is also topologically trivial in two spatial dimensions. The full Hamiltonian, for $v_1 \neq v_2$, is then a class A Chern insulator with a nonzero Chern number that is independent of the

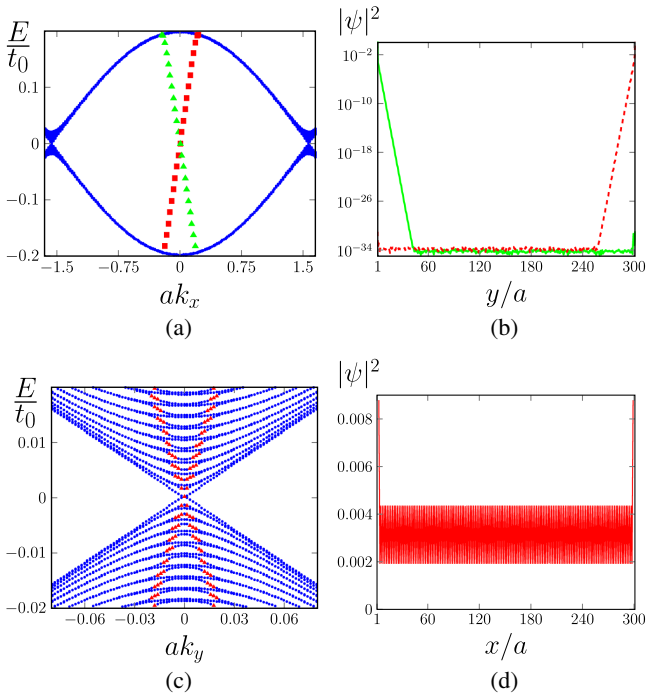

FIG. 1 (color online). Band structure and edge state wave functions of model I for different edge orientations. Edges along the y direction in (a) and (b): Localized edge states (red, green) coexist with zero modes in the bulk (blue). Edges along the x direction in (c) and (d): Because of energy and momentum overlap, hybridized edge states (red) coexist with the bulk states.

sign of m, so it belongs to the first class of models mentioned in the Introduction. Therefore, the system has to have chiral gapless edge states as well as a gapped bulk, independent of the orientation of the edge. The weak edge states must therefore be stabilized by the appearance of a small mass term. In fact, the same holds for disorder—the full Hamiltonian belongs to class A [1,2], in which the bulk states become localized. Because of the nonzero Chern number, the edge states cannot disappear and must therefore be stabilized by disorder. To confirm this expectation, we numerically analyze two-terminal transport in the system. All transport simulations are performed using the KWANT code [18]. We discretize the Hamiltonian on a square lattice of $L \times W$ sites and attach ideal leads in the x direction. This enables us to compute the scattering matrix

$$S = \begin{pmatrix} r & t \\ t' & r' \end{pmatrix}, \tag{3}$$

which we use to determine the conductance $G/G_0 = \mathrm{Tr} t^\dagger t$, $G_0 = e^2/h$ in the low bias voltage, low temperature limit. In the y direction, we either use hard wall boundary conditions (Hall bar geometry) or apply periodic boundary conditions to the states, $\psi(x, 0) = \psi(x, W)$, to access only the bulk contribution to transport (Corbino geometry). Here and in all other models, disorder is introduced as a random variation of the Fermi energy, drawn independently for each lattice site from the uniform distribution $[-\delta, \delta]$. As seen in Fig. 2(b), when the disorder strength δ increases, the conducting bulk states originating from H_2 localize, leaving behind only the quantized conductance of the edge. The phase diagram is obtained by performing transport simulations with periodic boundary conditions and in the presence of a mass term [Fig. 2(a)]. Starting from the gapless point, $m = \delta = 0$, both the addition of a mass term and disorder drive the system into a Chern insulating phase with $C = 1$.

Model II.—A gapped Chern insulator coupled to a Chern insulator at its critical point. In this model, we keep H_1 as before, but replace H_2 by a Hamiltonian of a quantum Hall state at the transition between two Chern numbers. This Hamiltonian is nothing but the Hamiltonian appearing in Eq. (2) with $\sigma_z \to -\sigma_z$ and $\mu = 2$. Here, the gapped H_2 belongs to class A with a Chern number of either zero or -1. Therefore, the full Hamiltonian is a class A Chern insulator with a Chern number changing from $C = 0$ to $C = 1$. In contrast to model I, here the edge states disappear as disorder is introduced since the system enters a $C = 0$ phase. The phase diagram of this model is shown in the Supplemental Material [20].

Model III.—A gapped Chern insulator coupled to a quantum spin Hall state at its critical point. In the previous models, both the gapped and the gapless Hamiltonian were subjected to localization by disorder. Now we choose an H_2 that does not get localized by weak disorder. Interestingly, we find that its coupling to the gapped Chern insulator makes it amenable to localization. We set H_2 as the Bernevig-Hughes-Zhang (BHZ) model for the quantum spin Hall effect [9],

$$H_2 = \begin{pmatrix} h(\mathbf{k}) & \Gamma(\mathbf{k}) \\ \Gamma^\dagger(\mathbf{k}) & h^*(-\mathbf{k}) \end{pmatrix}, \tag{4}$$

with

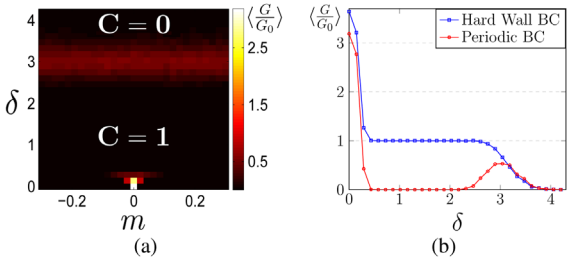

FIG. 2 (color online). (a) Disorder averaged bulk conductance of model I as a function of disorder strength δ and the gap-opening parameter m. Chern numbers of the two phases are shown. (b) Average conductance G/G_0, for $m = 0$, as a function of δ, for periodic (red line) and hard wall (blue line) boundary conditions; see Ref. [19] for simulation parameters.

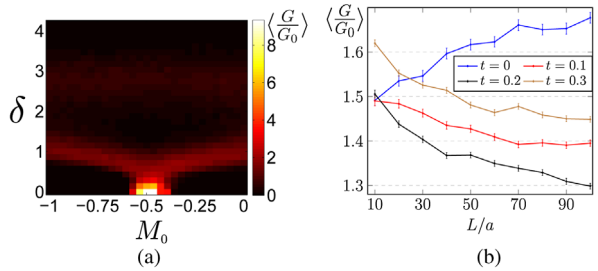

FIG. 3 (color online). (a) Disorder averaged bulk conductance of model III, as a function of M_0 and disorder strength δ. (b) Average bulk conductance for $M_0 = -1$ and $\delta = 0.95$, as a function of the system size L for different coupling strengths. The conducting region around $\delta = 1$ becomes localized as the system size is increased. See Ref. [23] for simulation parameters.

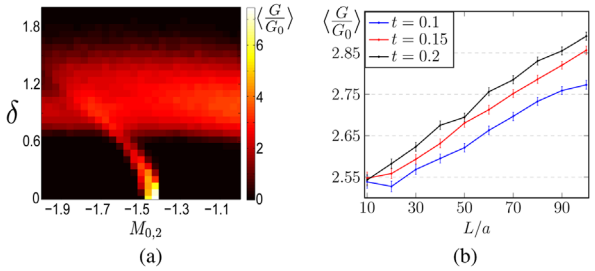

FIG. 4 (color online). (a) Disorder averaged bulk conductance of two coupled BHZ models, as a function of disorder strength δ and $M_{0,2}$. (b) Average bulk conductance for $\delta = 1$ and $M_{0,2} = -1.47$, as a function of the system size L for different couplings t. See Ref. [26] for simulation parameters.

$$h(\mathbf{k}) = [M_0 + 2M_2(1 - \cos k_x - \cos k_y)]\sigma_z + A\sigma_x \sin k_x + [C_0 + 2C_2(1 - \cos k_x - \cos k_y)]\sigma_0 - A\sigma_y \sin k_y,$$
$$\Gamma(\mathbf{k}) = \Delta(\sigma_0 \sin k_x + i\sigma_z \sin k_y) - i\Delta_0\sigma_y, \quad (5)$$

where the σ_i's act in the subspace of the E and H orbitals of the BHZ model. We choose M_0 such that H_2 is in a metallic region between two nontrivial quantum spin Hall phases (symmetry class AII). For the full model, we take H_1 as in Eq. (2), and a simple coupling Hamiltonian,

$$H_c = t\begin{pmatrix} 1 & i & 1 & i \\ 1 & i & 1 & i \end{pmatrix}. \quad (6)$$

Similar to Figs. 1(a) and 1(b), in the absence of disorder, bulk and edge modes coexist in the spectrum [20]. While H_2 is time-reversal symmetric, allowing for the existence of metallic phases in the presence of disorder, the coupled model belongs to class A, where weak disorder leads to localization. Seemingly, the phase diagram in the space of M_0 and disorder strength δ, depicted in Fig. 3(a), shows a metallic phase at finite disorder strength, reminiscent of that present in the BHZ model. A conductance scaling analysis [Fig. 3(b)] shows that it is metallic only in the decoupled case. When the coupling is turned on, the conductance decreases with system size, showing that the presence of the conducting region is caused by the finite size of the system. In accordance with Fig. 2(a), as the disorder strength is increased, the bulk states localize, leaving behind only the quantized conductance contribution of the edge states. This exemplifies the fact that both the topological and the localization properties depend on the symmetry class of the full Hamiltonian.

Model IV.—A gapped quantum spin Hall phase coupled to a quantum spin Hall phase at its critical point. We now consider both H_1 and H_2 to be BHZ models, Eqs. (4) and (5), with different mass terms, $M_{0,1}$ and $M_{0,2}$, respectively. We set H_1 to be in a topological phase and H_2 in a metallic region. This model can be directly implemented experimentally, for example with two coupled Hg(Cd)Te quantum wells, as proposed in Ref. [24]. Most directly, this model may be realized in such systems when one of the quantum wells is grown with a critical thickness [25] while the other well is chosen to be in a topologically nontrivial phase. Remarkably, the system may be driven to the gapless point (see Ref. [20]) by the application of voltage on the front and back gates even when the thickness of the two wells does not conform to this requirement.

We choose a coupling Hamiltonian $H_c = t(\sigma_0 + \sigma_z)\tau_0$, found in Ref. [24], to describe the experimentally accessible parameter regime. The Pauli matrices σ describe the space of the E and H orbitals, and τ parametrizes the spin degree of freedom. In the absence of disorder [20], we find features similar to the previous models, the system simultaneously hosting gapless modes in the bulk and on the edge. Like in model III, when $M_{0,2}$ is changed the bulk becomes insulating, but this time it is characterized by a different invariant, belonging to $\mathbb{Z}_2$ instead of the $\mathbb{Z}$ valued Chern number. The disordered case also shows a behavior different from the previous models. Since the full Hamiltonian belongs to class AII, weak antilocalization leads to the formation of a metallic phase at finite disorder strength; see Fig. 4(a). This is confirmed by the scaling analysis of Fig. 4(b). The experimental signature of this phase is the coexistence of helical edge modes and conducting bulk, which can be verified experimentally by performing conductance measurements in three-terminal devices with polarized leads. We elaborate on the experimental setup in the Supplemental Material [20].

Summary.—We have suggested a route to realizing unusual two-dimensional topological phases that simultaneously host gapless modes in the bulk and on the edges. We have found that the behavior of these phases in the presence of disorder can be extracted from the clean limit by analyzing their topological properties in the presence of an infinitesimal bulk gap. Finally, we have proposed a concrete physical realization of one such model, based on double Hg(Cd)Te quantum wells.

Financial support from the DFG (German-Japanese research unit "Topotronics"; priority program SPP 1666 "Topological insulators"), the Helmholtz Foundation (VITI), and the ENB Graduate School on Topological Insulators is gratefully acknowledged by T. P. and B. T. T. P. wants to thank P. Michetti for the interesting discussions and the Weizmann Institute for their hospitality. Y. B., I. C. F., and A. S. gratefully acknowledge support from the European Research Council under the European Union's Seventh Framework Programme (FP7/2007–2013)/ERC Project MUNATOP, the U.S.-Israel Binational Science Foundation, and the Minerva Foundation.

[1] A. P. Schnyder, S. Ryu, A. Furusaki, and A. W. W. Ludwig, Phys. Rev. B **78**, 195125 (2008).
[2] A. Kitaev, AIP Conf. Proc. **1134**, 22 (2009).
[3] X.-L. Qi and S.-C. Zhang, Rev. Mod. Phys. **83**, 1057 (2011).
[4] F. D. M. Haldane, Phys. Rev. Lett. **61**, 2015 (1988).
[5] C. L. Kane and E. J. Mele, Phys. Rev. Lett. **95**, 146802 (2005).
[6] L. Fu, C. L. Kane, and E. J. Mele, Phys. Rev. Lett. **98**, 106803 (2007).
[7] J. E. Moore and L. Balents, Phys. Rev. B **75**, 121306 (2007).
[8] L. Fu and C. L. Kane, Phys. Rev. Lett. **100**, 096407 (2008).
[9] B. A. Bernevig, T. L. Hughes, and S.-C. Zhang, Science **314**, 1757 (2006).
[10] M. König, S. Wiedmann, C. Brüne, A. Roth, H. Buhmann, L. W. Molenkamp, X.-L. Qi, and S.-C. Zhang, Science **318**, 766 (2007).
[11] M. Z. Hasan and C. L. Kane, Rev. Mod. Phys. **82**, 3045 (2010).
[12] D. Hsieh, Y. Xia, D. Qian, L. Wray, J. H. Dil, F. Meier, J. Osterwalder, L. Patthey, J. G. Checkelsky, N. P. Ong, A. V. Fedorov, H. Lin, A. Bansil, D. Grauer, Y. S. Hor, R. J. Cava, and M. Z. Hasan, Nature (London) **460**, 1101 (2009).
[13] Y. L. Chen, J. G. Analytis, J.-H. Chu, Z. K. Liu, S.-K. Mo, X. L. Qi, H. J. Zhang, D. H. Lu, X. Dai, Z. Fang, S. C. Zhang, I. R. Fisher, Z. Hussain, and Z.-X. Shen, Science **325**, 178 (2009).
[14] D. Hsieh, Y. Xia, L. Wray, D. Qian, A. Pal, J. H. Dil, J. Osterwalder, F. Meier, G. Bihlmayer, C. L. Kane, Y. S. Hor, R. J. Cava, and M. Z. Hasan, Science **323**, 919 (2009).
[15] S. Matsuura, P.-Y. Chang, A. P. Schnyder, and S. Ryu, New J. Phys. **15**, 065001 (2013).
[16] R. Queiroz and A. P. Schnyder, Phys. Rev. B **89**, 054501 (2014).
[17] X.-L. Qi, Y.-S. Wu, and S.-C. Zhang, Phys. Rev. B **74**, 085308 (2006).
[18] C. W. Groth, M. Wimmer, A. R. Akhmerov, and X. Waintal, New J. Phys. **16**, 063065 (2014).
[19] The lattice size is $L \times W = 80 \times 80$, and Hamiltonian parameters are $\mu = v_1 = 1$, $t_1 = 0$, $v_2 = 0.2$, and $t = 0.1$. Each point is obtained by averaging over 100 independent realizations of disorder.
[20] See Supplemental Material at http://link.aps.org/supplemental/10.1103/PhysRevLett.114.136801 for more details on the analysis of models II, III and the experimental realization, which includes Refs. [21, 22].
[21] D. G. Rothe, R. W. Reinthaler, C.-X. Liu, L. W. Molenkamp, S.-C. Zhang, and E. M. Hankiewicz, New J. Phys. **12**, 065012 (2010).
[22] C. Liu, T. L. Hughes, X.-L. Qi, K. Wang, and S.-C. Zhang, Phys. Rev. Lett. **100**, 236601 (2008).
[23] The lattice size in Fig. 3(a) is $L \times W = 80 \times 80$, and Hamiltonian parameters are $\mu = v_1 = 1$, $t_1 = 0.4$, $t = 0.2$, $A = M_2 = 1/4$, $\Delta_1 = 0.1$, $\Delta_0 = 0.05$, $C_0 = -0.02$, and $C_2 = 0$. Each point is obtained by averaging over 50 independent realizations of disorder for Fig. 3(a). In Fig. 3(b), the aspect ratio is fixed to $L/W = 1$ and 2000 disorder realizations are considered.
[24] P. Michetti, J. C. Budich, E. G. Novik, and P. Recher, Phys. Rev. B **85**, 125309 (2012).
[25] B. Buttner, C. X. Liu, G. Tkachov, E. G. Novik, C. Brune, H. Buhmann, E. M. Hankiewicz, P. Recher, B. Trauzettel, S. C. Zhang, and L. W. Molenkamp, Nat. Phys. **7**, 418 (2011).
[26] All parameters of the two BHZ models are the same as in model III, except for $M_{0,1} = -0.8$. The coupling strength is $t = 0.15$. In Fig. 4(a), we averaged over 50 realizations, while 2000 are used in Fig. 4(b). The phase diagram is computed for a lattice of $L \times W = 80 \times 80$ sites, while the conductance scaling is done at a constant aspect ratio of $L/W = 1$.